EXPERIMENTAL MEASUREMENTS ON NON-NEWTONIAN AND DRAG REDUCTION FLOWS IN PIPES

A. VERBA, M. H. EMBABY* and I. ANGYAL

Department of Mechanical Engineering for the Chemical Industry,
Technical University, H-1521 Budapest

Received February 12, 1982

Summary

A laboratory setup was designed for experimental study of non-Newtonian and drag reducing fluid flow in a square cross section pipe. Aqueous solutions of carboxymethyl cellulose (CMC) in water were used as the non-Newtonian fluids while dilute solutions of polyethylene oxide (PEO) in water as the drag reducing fluids. An injection technique was used to overcome the pump degrading effects on the PEO solutions.

A turbometer was used for flow rate measurements, a pressure transducer for pressure measurements, Pitot tubes for velocity measurements and Preston tubes for wall shear stress measurements.

The performance and calibration of the previous devices are presented in this paper with some results compared with theory.

Introduction

Pipe flow regimes, widely met in practice, include non-Newtonian and drag reduction flow regimes.

Non-Newtonian fluids have been defined and classified by many authors, [1], with respect to the shear stress–shear rate correlation. These fluids include the common "power law" fluids. The shear stress–shear rate correlation for a power law fluid, in one-dimensional simple shear flow, reads:

$$\tau = \eta(\gamma)^n \tag{1}$$

where η and n are rheological parameters of the fluid. For the (CMC) solutions, used in the present experiments, a rotary viscometer was used to determine the shear stress–shear rate correlations. The data fitted, reasonably, the power law model. Corrections have been made for the non-Newtonian effects on the rotary viscometer data [2].

Most of the drag reducing fluids are combinations of Newtonian solvents and long-chain polymers of relatively low concentrations. The drag reducing fluids have nearly the same viscosity as the solvents [3].

* Permanent address: Faculty of Engineering and Technology, Shibin El-Kom, Egypt

Drag reduction may be plotted by correlating the gross flow data using Prandtl–Karman coordinates as shown in Fig. 15. Three flow regimes are seen to exist. The Newtonian flow regime represents the gross flow data of the solvent alone. The polymer solution follows that line to a certain "onset condition" (Re $\sqrt{f}$)* where the drag reduction effect begins to appear. Thus for the polymer solution, at a certain concentration, there are two flow characteristics; an onset wall shear stress τ_w^* and a slope increment Φ. The maximum drag reduction asymptote represents the maximum drag reduction possible for any polymer solution. This asymptote is independent of the polymer concentration or characteristics.

In the present experiments, the common PEO-water solutions have been used as the drag reducing fluids.

Setup description and measurements

Figure 1 shows the experimental setup which consists of a 2.4 × 2.4 cm test pipe, recirculating pump, measuring systems and polymer solution injection system. The following section concerns the performance of the previously mentioned systems.

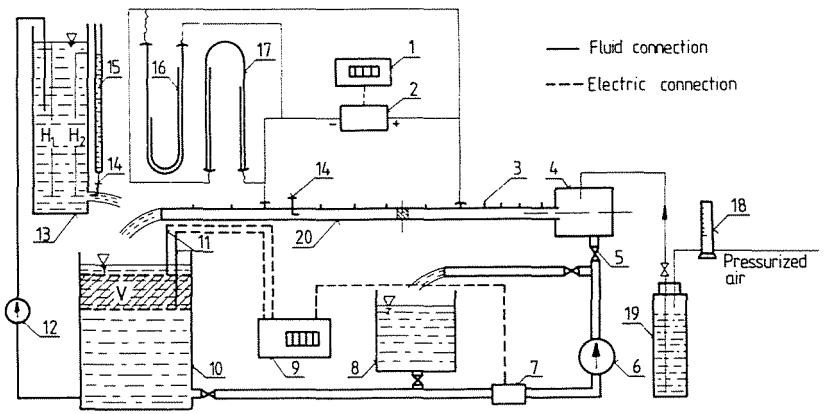

Fig. 1. Experimental setup

1 — Digital multimeter
2 — Pressure transducer
3 — Pressure tap
4 — Entrance chamber
5 — Control valve
6 — Circulating pump
7 — Turbometer
8 — Secondary tank
9 — Pulse counter
10 — Main circuit tank
11 — Sensing conductors
12 — Pump
13 — Pitot tube calibration tank
14 — Pitot tube
15 — Piezometer tube
16 — Mercury manometer
17 — Water manometer
18 — Rotameter
19 — Concentrated polymer solution tank
20 — Test pipe

i. *Polymer solution preparation*

CMC solutions were prepared by adding the dry polymer to the water, with hand stirring, at a relatively high concentration. These solutions were stored for 24 h, and then diluted to the required concentration.

PEO, $M_w = 5 \times 10^6$, drag reducing solutions were prepared by first suspending the dry polymer in a few milliliters of alcohol to prevent agglomerate formation. This suspension was added to water, with gentle stirring, to get a certain concentration and the solution was stored for 48 h before use.

ii. *Pump degradation tests and injection system*

The degrading effect of the centrifugal pump (6) in Fig. 1, on polymer solution PEO was tested as follows. The pump performance characteristics —power, head, efficiency and discharge—were measured with polymer solutions through successive pumping strokes. During one stroke, tank (10) was used as a suction tank while tank (8) as a delivery tank. The circuit was reversed in the second stroke and so on. It was observed (Fig. 2), that the Newtonian performance intervened after about 10 strokes. The number of strokes represents how many times the solution passed through the pump.

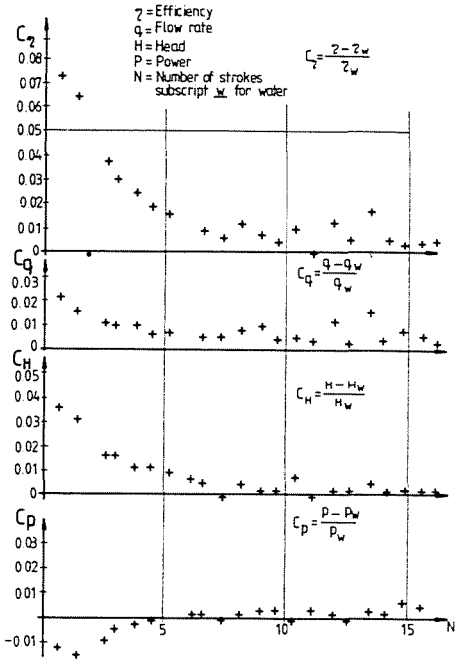

Fig. 2. The degradation effect of the centrifugal pump with PEO (M $5 \cdot 10^6$) solution $c = 12$ ppm

Y. Goren [4] suggested an injection system of concentrated solutions of PEO, $M_w = 4 \times 10^6$ in the wall region of a circular pipe using a gear pump. With that system a maximum drag reduction (mdr) was obtained at 10 ppm concentration and $\mathrm{Re} = 1.5 \times 10^5$.

In conformity with the above mentioned technique, and also to avoid pump degrading effects, an injection system was used in the present experiments. The concentrated PEO solutions were injected at the test pipe square cross section entrance with pressurized air. The system is shown in Fig. 1, parts 4, 18 and 19. The required flow concentration was adjusted via the turbometer — in the main circuit (7) — and the calibrated rotameter (18).

An effective drag reduction could be obtained using the above mentioned system as seen in Fig. 15. The maximum drag reduction achieved in the present experiments was at $c = 20$ ppm. During experiments, when injection stopped, the recorded pressure drops immediately increased to their former values with solvent alone, before injection. This check also held at the highest concentration — 20 ppm — used.

iii. *Flow rate measuring system*: (7), (9) and (11) in Fig. 1

A 50 mm bore diameter type HB 50/70 calibrated turbometer was used for flow rate measurements. Dimensional analysis for correlating calibration data to power law fluid flow in a turbometer has led to:

$$Q/\omega D_b^3 = f(\omega^{2-n} D_b^2/(\eta/\rho)) \tag{2}$$

a correlation to be reduced to that for Newtonian flow [5] by setting $n = 1$ and $\eta = \mu$. Two calibration circuits were used. The first circuit, with suction from tank (8) and delivery to tank (10) in Fig. 1 resulted in inaccurate and irreproducible results as indicated by the hollow points in Fig. 3. This may be attributed to the relatively high electrical conductivity of the solutions.

When the second calibration circuit was used, with suction from tank (10) and delivery to tank (8), better results were obtained, shown in full points in Fig. 3.

It may be concluded that the turbine performance curve for Newtonian fluids can be used for non-Newtonian "power law" fluids using the general form of the turbine Reynolds number $\mathrm{Ret} = \omega^{2-n} D_b^2/(\eta/\rho)$.

iv. *Velocity measurements*

The use of Pitot tubes for velocity measurements, in drag reduction flows, was studied by several authors [6–8]. The reports showed the viscoelastic effects of those fluids to cause anomalous measurements. In order to study the viscoelastic effects in the present study, a jet calibration system ((13), (14) and (15)), was used (Fig. 1). The nozzle diameter was 1 cm and the maximum

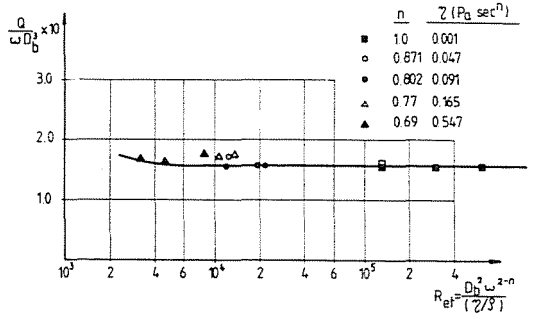

Fig. 3. Turbometer characteristics with Newtonian and non-Newtonian fluids

available head on the tank (13) was 100 cm allowing a calibration velocity range of 1.5 to 4 m/s. The calibrated Pitot tube was 1 mm diam.

In order to correlate the calibration data, the head H_1 inside the calibration tank (13) was taken as a reference. The nozzle entrance was carefully rounded and thus the nozzle was assumed to cause no losses. Also a hat profile was assumed after the nozzle.

With the above assumptions, the theoretical velocity is:

$$u_{\text{th}} = \sqrt{2gH_1}\,.$$

The velocity read off the Pitot tube:

$$u_{\text{P}} = \sqrt{2gH_2}$$

where H_2 is the head read off the Pitot tube. The actual to theoretical velocity ratio $\dfrac{u_{\text{P}}}{u_{\text{th}}} = \sqrt{\dfrac{H_2}{H_1}}$ plotted against the velocity head is seen in Figs 4 and 5,

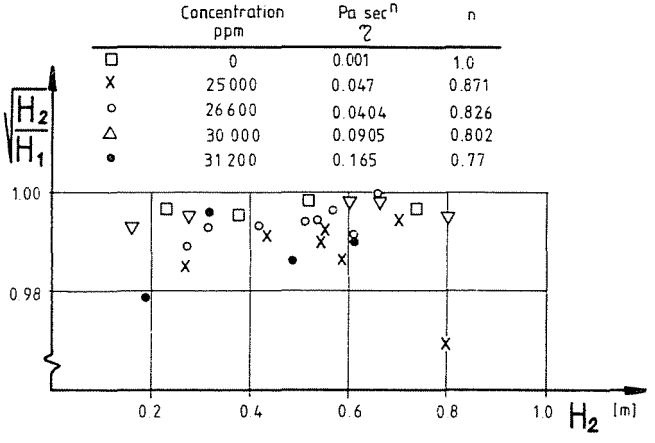

Fig. 5. Pitot tube calibration results for PEO solutions

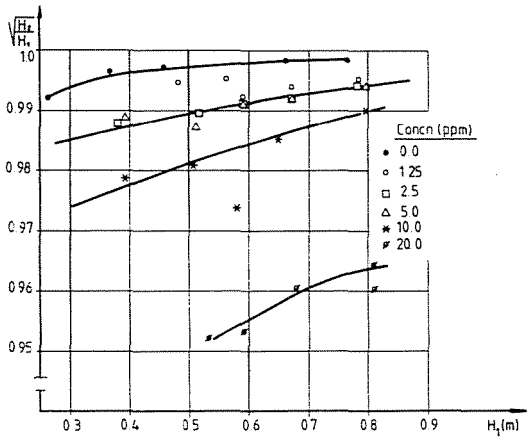

Fig. 4. Pitot tube calibration results for non-Newtonian (CMC) solutions

showing the calibration data for the non-Newtonian and drag reducing fluids, respectively. Both figures indicate more anomalous measurements with increase of the polymer concentration. Also, the figures show that the PEO solutions exhibit more anomalous measurements, hence a higher viscoelasticity, than do CMC solutions. Figures 6 and 7 show the measured velocity profiles, under flow conditions, for now-Newtonian and drag reducing fluids, resp. The figures also indicate a reasonable agreement with theory [9–10] in spite of the above mentioned deficiencies.

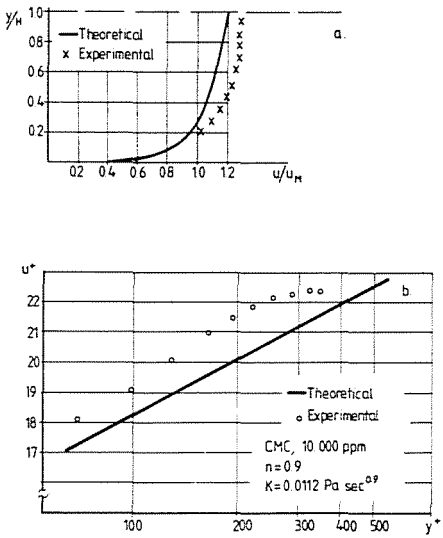

Fig. 6. Experimental velocity profile compared with theory [9] for non-Newtonian (CMC) solution

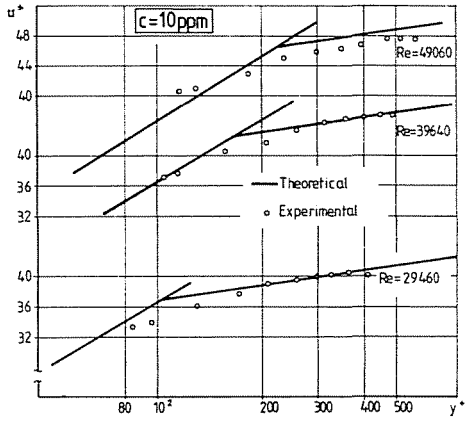

Fig. 7. Experimental velocity profile compared with theory [10] for PEO solution

v. *Wall shear stress measurements*

The Pitot tubes were used as "Preston tubes" by resting on the test pipe wall [11]. These measurements were only carried out with drag reduction flows due to the longer entrance lengths with those flows [9–10].

Two tubes, located at different positions far enough from the entrance, were calibrated at different wall shear stresses for PEO solutions at different concentrations. The calibration data were plotted using the coordinates by Patel [11] shown in Fig. 8.

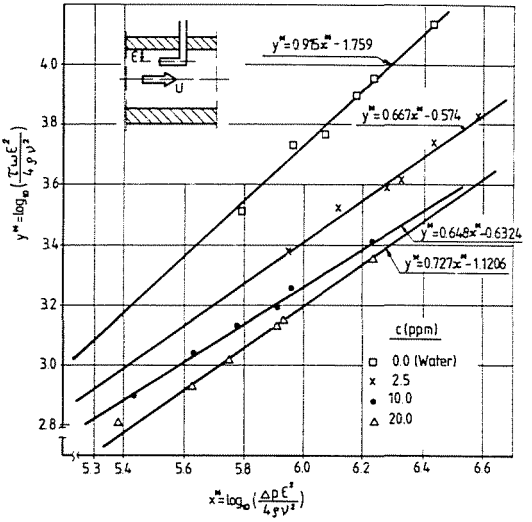

Fig. 8. Preston tube performance with different PEO polymer concentrations

Figure 8 shows an interesting "drag reduction depicting" feature. For a certain concentration: as the wall shear stress, i.e., y^* increases, the performance tends to the maximum drag reduction asymptote represented by the 20 ppm line in the figure. On the other hand, as y^* decreases the performance tends to the Newtonian one. Thus, an "onset" wall shear stress is obtained at the intersection of the performance line, for a certain concentration and the Newtonian line. Figure 9 shows the "onset" wall shear stresses, obtained as mentioned above, compared with those obtained from pipe gross flow, $1/\sqrt{f} - \mathrm{Re}\sqrt{f}$, data.

Figures 10 and 11 show some measurements of the wall shear stresses, i.e. f distributed along the pipe compared with theory.

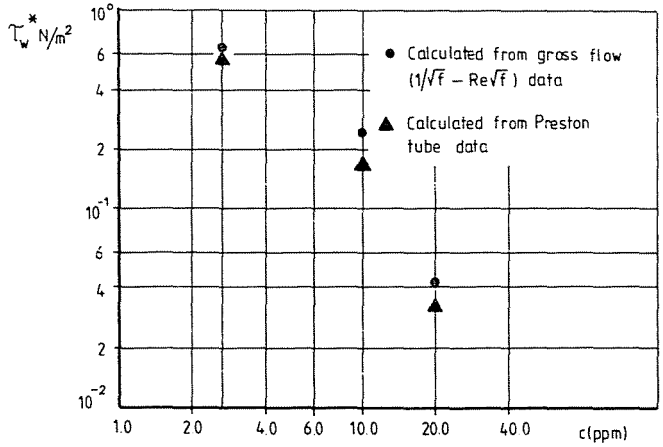

Fig. 9. Onset wall shear stress predictions from experimental data

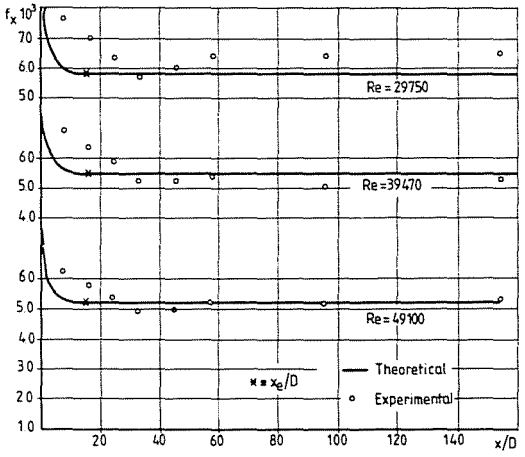

Fig. 10. Comparison between theoretical [10] and experimental friction factor distribution — measured with Preston tube — for water

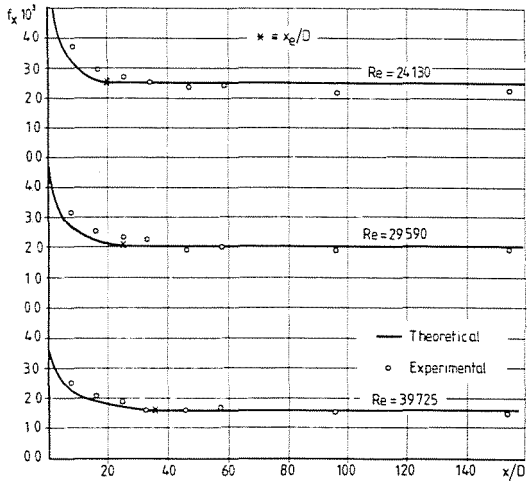

Fig. 11. Contd.; $c = 10$ ppm

vi. *Pressure measurement system*

Fifteen pressure tap holes 2 mm diameter were distributed along the test pipe and connected to a differential pressure transducer 0.0 – 0.6 bar through a manifold. The transducer was connected to a digital multimeter and calibrated for low and high pressure differentials using the water and mercury manometers shown in Fig. 1.

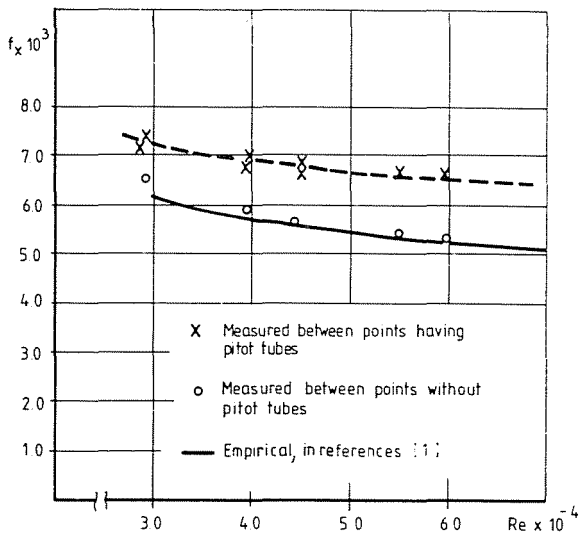

Fig. 12. The measured increase of the friction factor due to the Preston tubes

During pressure measurements, the Pitot tubes were set to rest on the test pipe wall. The pressure losses due to those tubes were studied under Newtonian flow conditions. The pressure drops, hence the friction factors, were measured simultaneously at two different sections along the test pipe. Both sections were at a distance $X/D > 25$ from the entrance, i.e., in the fully developed zone [9]. The section containing Pitot tubes showed higher friction factors as shown in Fig. 12. Based on these measurements the pressure loss ΔP_P due to the Pitot tube was approximately correlated using a loss factor ξ_p as:

$$\Delta P_p = \xi_p \times 0.5\, \rho U_M^2 . \tag{3}$$

Figure 13 shows the variation of the factor ξ_p with Re and the average value ξ_{pav} indicated in dotted line. Figure 14 shows the pressure distribution at different Reynolds numbers compared with theory [9]. In this figure, correction factor ξ_{pav} was used in plotting the measured pressure differentials. For non-Newtonian and drag reduction flows the same correction factor ξ_{pav} was assumed.

Figure 15 shows the gross flow data plotted in Prandtl–Karman coordinates for PEO solutions taking the previously discussed Pitot tube losses into consideration.

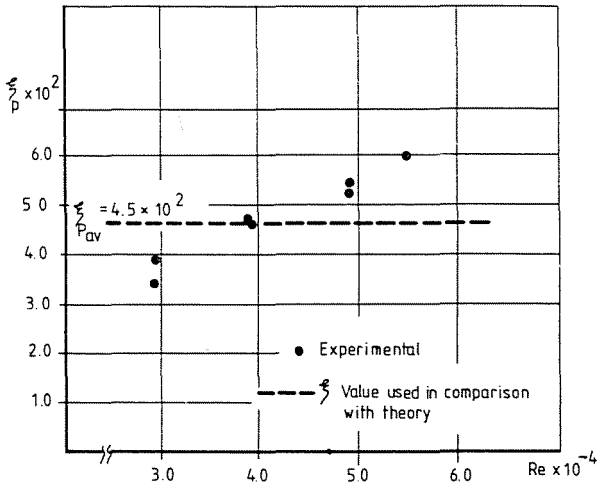

Fig. 13. Pressure drop correction factor ξ_p at different Re values

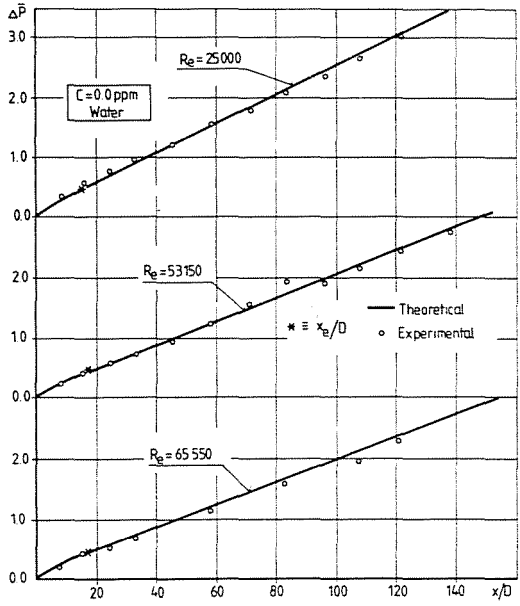

Fig. 14. Comparison between theoretical [9] and experimental pressure distribution for water (Newtonian)

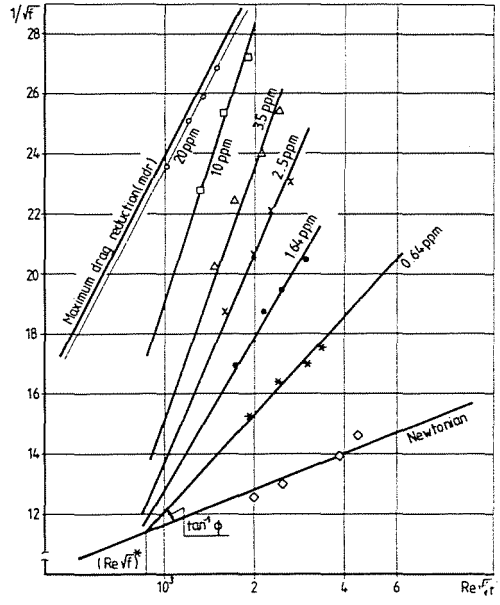

Fig. 15. Experimental gross flow data for PEO solutions

List of symbols:

c concentration ppm;
D, D_b hydraulic diameter, turbometer bore diameter resp;
f friction factor $f = \tau_w / 0.5 \rho U_M^2$;
H half duct width;
H_1, H_2 head in the discharge tank, head read by the impact tube, resp.;
n flow behaviour index for non-Newtonian fluids;
ΔP_p, ΔP_i pressure loss due to Pitot tube resistance, difference between total and static pressures for Preston tube measurements;
Q volume flow rate;
Re Reynolds number;
$\mathrm{Re} = U_M D / \nu$ for Newtonian and drag reduction flows, and
$\mathrm{Re} = \rho U_M^{2-n} D^n / 8^{n-1} \cdot \eta \cdot (0.2121/n + 0.6766)^n$ for non-Newtonian flows;
$\mathrm{Ret} = \omega^{2-n} D_b^2 / (\eta/\rho)$ turbine Reynolds number;
u, U_M, u_τ axial, average velocity, shear velocity;
$u^+ = u/u_\tau$ dimensionless velocity
x, x^* axial distance, abscissa of Preston tube calibration plot, Fig. 8;
x_e entrance length;
y, y^* distance from pipe wall, ordinate of Preston tube calibration plot, Fig. 8;
$y^+ = \dfrac{y^n u_\tau^{2-n}}{\eta/\rho}$ dimensionless distance
γ shear rate;
η consistency index for non-Newtonian fluids;
Φ slope increment for drag reduction flows;
μ dynamic viscosity of solvent in case of drag reduction flows;
ν kinematic viscosity of solvent;
ρ density;
τ_w, τ_w^* wall shear stress, onset wall shear stress for drag reduction flows, resp.,
ω rotor angular speed;
ε Preston tube center-line distance from pipe wall, Fig. 8;
ξ_p, ξ_{pav} Pitot tube pressure loss factor, average loss factor, resp., Eq. (3);

References

1. SKELLAND, A. H. P.: Non-Newtonian Flow and Heat Transfer. J. Wiley, New York 1967.
2. TROUILHET, von Y.—WIDMER, F.: Technisches Messen. atm, Heft 5, 167—171, 1978.
3. VIRK, P. S.: AICHE J., Vol. 21, No 4, 625—656, 1975.
4. GOREN, Y.: Trans. ASME, J. of Basic Eng., p. 814—822, December 1967.
5. DOEBELIN: Measurement System Application and Design, Mc Graw Hill, 1966. pp. 475—478.
6. FRIEHE, C. A. et al.: The Use of Pitot-Static Tubes and Hot-Film Anemometers in Dilute Polymer Solutions. Symposium in Viscous Drag reduction, pp. 281—296, Ed. Sc. Wills, 1969.
7. SMITH, K. A. et al.: Ch. Eng. Sc., Vol. 22, pp. 619—626, 1967.
8. ASTARITA, G. et al.: AICHE J. vol. 12, No. 3, pp. 478—484, 1966.
9. EMBABY, H.—VERBA, A.: Theoretical and Experimental Studies of the Developing Turbulent Non-Newtonian Flow in a Pipe; submitted at the XV. Biennial Fluid Dynamics Symposium, 6—12th Sept. 1981 (Poland).
10. EMBABY, M. H.: Entrance Zone Properties of Non-Newtonian and Drag Reduction Turbulent Pipe Flows. Ph. D. Thesis. Budapest, 1981.
11. PATEL, V. C.: J. Fluid Mech., Vol. 23, pt. 1, pp. 185—208, 1965.

DR. Attila VERBA
István ANGYAL } H-1521 Budapest
Mohamed Hamed EMBABY Faculty of Engineering and Technology, Shibin El-Kom, Egypt